Evaporation dynamics of nanodroplets and their anomalous stability on rough substrates

Yawei Liu and Xianren Zhang*
Division of Molecular and Materials Simulation, State Key Laboratory of Organic-Inorganic Composites, Beijing University of Chemical Technology, Beijing 100029, China
(Received 24 April 2013; published 26 July 2013)

Nanodroplets sitting on substrates in an open system are usually assumed to be thermodynamically unstable, and will eventually either evaporate or grow. However, as a counterpart of nanodroplets, nanobubbles located at the solid-liquid interface were recently demonstrated by numerous experiments to be unexpectedly stable. The accumulated evidence for the existence of stable nanobubbles poses a question of whether nanodroplets are stable. In this work we revisit the stability of nanodroplets upon smooth and rough substrates, concentrating on their evaporation dynamics. On smooth substrates, the droplets evaporate generally in the constant contact angle (CCA) mode, with a contact angle nonmonotonously depending on the fluid-substrate interaction, while on rough substrates, the droplets evaporate in the constant contact line (CCL) mode or the CCL-CCA mixed mode. Our results indeed predict the existence of stable nanodroplets on rough substrates: In situations where the contact line is pinned and the vapor is supersaturated but at a low level of supersaturation, nanodroplets are found to be anomalously stable. The stability of nanodroplets can be interpreted within the framework of the classical nucleation theory.

DOI: 10.1103/PhysRevE.88.012404 PACS number(s): 68.08.De, 68.03.Fg, 64.60.qe, 61.20.Ja

I. INTRODUCTION

A sessile liquid droplet in an open system is expected to be thermodynamically unstable, and will eventually either evaporate under undersaturation or grow under supersaturation. The evaporation dynamics of droplets upon substrates, which is related to the wetting properties of the substrates [1,2], is of technological importance for coating, printing, electronic cooling, and other applications [3–7].

A more fundamental question is the stability of nanodroplets. A simple thermodynamics consideration using the Young-Laplace equation shows that, if nanodroplets are of a curvature radius in the nanometer range, the high internal pressures will lead to their rapid evaporation. However, as a counterpart of nanodroplets, nanobubbles located at the solid-liquid interface were recently demonstrated by numerous experiments to be unexpectedly stable [8–12]. Nanobubbles, although they appear to be forbidden by the high internal Laplace pressure, are commonly found on hydrophobic solid surfaces in solution opened to the air, and their lifetime is at least of the order of hours or days [13–15]. The accumulated evidence for the existence of stable nanobubbles, therefore, poses a question of whether nanodroplets are stable.

Inspired by the existence of stable nanobubbles, in this work we revisit the stability of nanodroplets upon smooth and rough substrates from the aspect of evaporation dynamics. After the pioneering work on the coffee ring effect [16], the mechanisms of droplet or solution evaporation have been extensively studied, both experimentally and theoretically [17–23]. Most of these studies dealt with the evaporation dynamics for large droplets sitting on substrates, with a size of at least several micrometers. Evaporating large droplets are found to exhibit different evaporation modes [24–28] such as the constant contact angle mode (CCA mode) with a shrinking contact line, the constant contact line mode (CCL mode) with a decreasing contact angle, and the mixed mode with a CCL-CCA transition. For droplets in the nanoscale, however, evaporation dynamics is difficult to investigate experimentally owing to the real-time and spatial resolution limitations of monitoring techniques. More complicatedly, the intermolecular forces between the solid and the fluid would influence the shape of nanodroplets near the three-phase contact line, and the nanoscale roughness of substrates inevitably affects the shrink and the spread of the contact line. As a result, the evaporation dynamics may change for droplets with a size down to the nanoscale, and thus affects the droplet stability.

In this work, we investigate the evaporation dynamics of nanodroplets sitting on smooth and rough substrates, respectively, using the kinetic lattice density functional theory (KLDFT) [29–31]. Different evaporation modes are observed on different substrates here. For nanodroplets upon smooth substrates, generally, they evaporate in the CCA mode but with a contact angle nonmonotonously depending on the fluid-substrate interaction, while for nanodroplets upon rough substrates, they evaporate in the CCL mode or CCL-CCA mixed mode, and in general ultimately disappear. However, if the droplets are exposed to a suitable vapor supersaturation and triple contact lines are pinned, nanodroplets would become stable.

II. METHOD

A. KLDFT

The method of KLDFT within the framework of mean field theory used in this work follows that of Monson [29]. The method has been successfully used to model fluid diffusion in confined spaces [29,31], the rupture of liquid bridges [30], and the stability of nanobubbles [32]. The theory gives an approximation to the time evolution of the density distribution averaged over an ensemble of configurations in the lattice gas model. The local density $\rho_i(t)$ at site i and time t can be written as

$$\rho_i(t) = \langle n_i \rangle_t = \sum_{\{n\}} n_i P(\{n\}, t), \quad (1)$$

*zhangxr@mail.buct.edu.cn

where $P(\{n\},t)$ is the probability of observing an occupancy configuration $\{n\}$ at time t. The evolution equation for the local density can be expressed as

$$\frac{\partial \rho_i(t)}{\partial t} = -\sum_j J_{ij}(t), \tag{2}$$

where $J_{ij}(t)$ is the net flux from site i to site j. In a mean field approximation [29], $J_{ij}(t)$ is given by

$$J_{ij}(t) = w_{ij}\rho_i(1-\rho_j) - w_{ji}\rho_j(1-\rho_i), \tag{3}$$

where w_{ij} is the transition probability for transitions from site i to site j. Thus Eq. (2) can be written as [29]

$$\frac{\partial \rho_i(t)}{\partial t} = -\sum_a [w_{i,i+a}\rho_i(1-\rho_{i+a}) - w_{i+a,i}\rho_{i+a}(1-\rho_i)], \tag{4}$$

where $w_{ij} = w_0 \exp(-E_{ij}/kT)$ with $E_{ij} = \{ {}^{0,\quad E_j < E_i}_{E_j - E_i,\ E_j > E_i}$, $E_i = -\varepsilon \sum_a \rho_{i+a} + \phi_i$, w_0 the jump rate in the absence of interactions, ε the nearest neighbor interaction strength for fluid, and $\phi_i = \sum_{j\neq i} \varepsilon_{sf}$ representing the sum of the fluid-solid interaction exerted on the site i. Euler's method was used to solve Eq. (2), and thus $\rho_i(t+\Delta t) = \rho_i(t) + \Delta t \sum_j J_{ij}(t)$ with $w_0 \Delta t$ being set to 0.1 to ensure the acceptable accuracy of the method. Calculations were performed at a reduced temperature of $T = k_B T/\varepsilon = 1.0$ with $\varepsilon = 1.0$, and hereafter all quantities reported in this work are expressed in their reduced units.

B. Calculation details

In this work, we employed a cubic box of 130 lattice spacings in three directions. A solid substrate with a thickness of 3 was placed on the bottom of the box, and in the other directions but far from the nanodroplet, a reservoir was also imposed to maintain the given chemical potential of the bulk solution. The relationship between chemical potential and relative humidity (RH) is given by $\mathrm{RH} = \exp[(\mu - \mu_C)/k_B T]$ with $\mu_C = -3.00$. For each calculation, first a metastable vapor state at the given temperature and chemical potential was obtained through a lattice density functional theory (LDFT) calculation. Then, a hemispherical droplet with the given volume was placed on the top of the substrate by setting the local density of the fluid lattice sites inside the droplet to 1.0, while the density of sites outside the droplet remained unchanged. The volume of the droplet is calculated by considering only the liquid lattice sites ($\rho_i > 0.5$).

III. RESULTS AND DISCUSSION

A. Evaporating nanodroplets on smooth substrates

We first considered the evaporation dynamics of nanodroplets sitting on smooth substrates, concentrating on the influence of the fluid-substrate interaction ε_{sf}. Note that ε_{sf} reflects the chemical nature of substrates and thus determines the macroscopic contact angle: $\varepsilon_{sf} < 0.5$ means the hydrophobic substrate with a contact angle of $\theta > \pi/2$ and $\varepsilon_{sf} > 0.5$ corresponds to the hydrophilic substrate with a contact angle of $\theta < \pi/2$. For each value of ε_{sf}, we fixed the initial volume of droplets to about 10 000, and the evaporation dynamics were determined with KLDFT at a given chemical potential of $\mu = -3.35$, corresponding to a RH of 70%.

In Fig. 1, we give typical morphologies and the evolutions of nanodroplet contact angles for different values of ε_{sf}. In general, for nanodroplets on smooth substrates, their evaporation dynamics is always in CCA mode, regardless of ε_{sf} [see Figs. 1(a)–1(e)]. However, as shown in Fig. 1(e), the contact angle shows a nonmonotonous dependence on the fluid-substrate interaction ε_{sf}.

As expected, Fig. 1 shows that the droplets present a contact angle of $\theta > \pi/2$ on hydrophobic substrates and a contact angle of $\theta < \pi/2$ on hydrophilic surfaces. However, an interesting morphology is observed in the case of $\varepsilon_{sf} = 1.1$ [see Fig. 1(c)]. At the early stage of evaporation, the strong fluid-substrate attraction induces the formation of a patch of monolayer liquid film on which the droplet sits, changing the evaporating nanodroplet into a straw-hat-like shape. The two

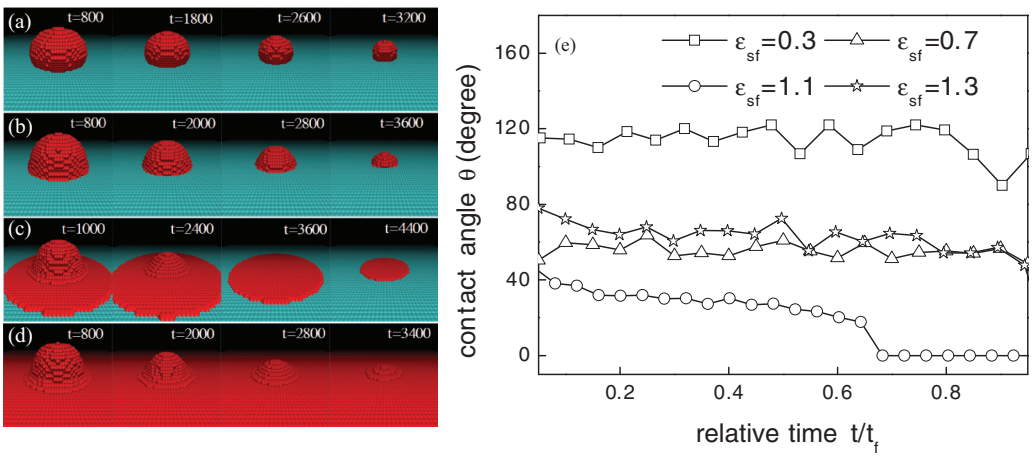

FIG. 1. (Color online) Time evolution of evaporating droplets upon smooth substrates. Typical snapshots of nanodroplets on different substrates: (a) $\varepsilon_{sf} = 0.3$, (b) $\varepsilon_{sf} = 0.7$, (c) $\varepsilon_{sf} = 1.1$, and (d) $\varepsilon_{sf} = 1.3$. The solid sites are shown in blue, the liquid sites are shown in red, and sites occupied by vapor are not shown for clarity. (e) The contact angle as a function of relative time t/t_f, with t_f the lifetime of nanodroplets. Note that the contact angles in the cases of $\varepsilon_{sf} = 1.1$ and 1.3 are measured as the angle at which the droplets meet the liquid film.

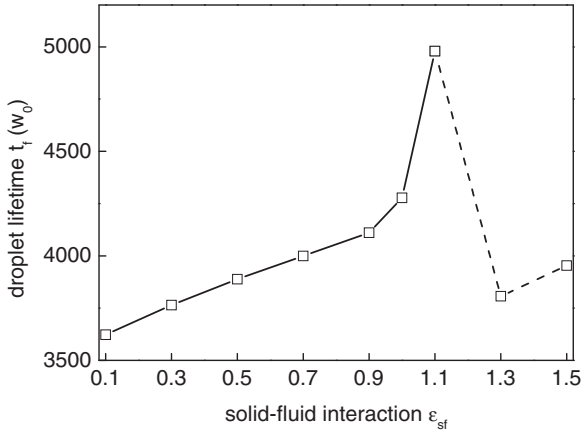

FIG. 2. The lifetime t_f of evaporating droplets upon smooth substrates as a function of ε_{sf}. The dashed line for the cases of $\varepsilon_{sf} > 1.1$ indicates that the preexisting liquid monolayer remains stable during the evaporation process.

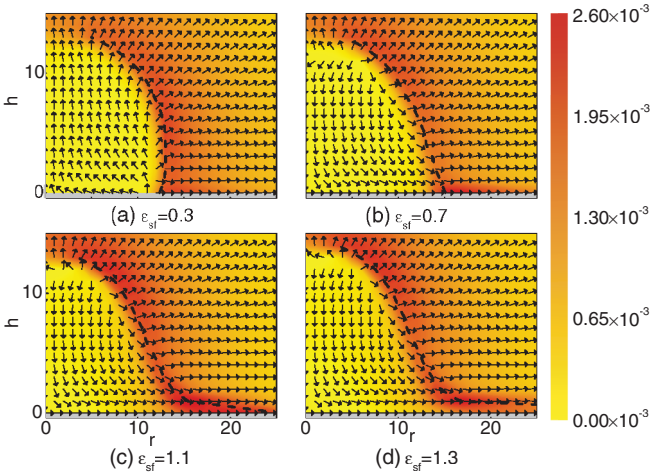

FIG. 3. (Color online) The flow field distributions at $t = 1000$ for evaporating droplets upon different smooth substrates: (a) $\varepsilon_{sf} = 0.3$, (b) $\varepsilon_{sf} = 0.7$, (c) $\varepsilon_{sf} = 1.1$, and (d) $\varepsilon_{sf} = 1.3$. The color code represents the flow rate, the arrow represents the flow direction, and the black dashed line represents the vapor-liquid interface.

parts of the droplet (the liquid film patch and the droplet on the liquid film) are found to evaporate in different modes: The upper droplet evaporates continuously in CCA mode [see Fig. 1(e)] and disappears first, while the film evaporates slowly and lasts for a much longer time. At the situation of $\varepsilon_{sf} = 1.3$, the liquid film is again formed and fully covers the substrate [Fig. 1(d)]. Different from the case of $\varepsilon_{sf} = 1.1$, the preexisting film remains stable during the whole evaporation process. In general, for $\varepsilon_{sf} > 1.0$, the preadsorbed film significantly affects the contact angle and therefore the evaporation dynamics.

Figure 2 shows the corresponding lifetime of nanodroplets. For $\varepsilon_{sf} < 1.0$, the droplet lifetime increases slightly with ε_{sf}. For ε_{sf} ranging from 1.0 to 1.1, the droplet lifetime shows a rapid increase and reaches a maximum at $\varepsilon_{sf} = 1.1$. The sharp increase of droplet lifetime can be interpreted rationally by the slow dynamics for the evaporation of the liquid film for a droplet at $\varepsilon_{sf} = 1.1$. When ε_{sf} increases further, the lifetime of droplets that sit upon the stable liquid film decreases sharply, and then remains nearly fixed. In other words, the lifetime of nanodroplets on smooth substrates is limited even though ε_{sf} is sufficiently large, particularly because the preexisting liquid film for $\varepsilon_{sf} > 1.0$ blocks the influence from the substrates. The nearly same contact angle for $\varepsilon_{sf} > 1.0$ [see Fig. 1(e)] also confirms the block effect. Therefore, we conclude that the strong attraction from the substrates alone cannot stabilize the nanodroplets, even though ε_{sf} is increased to 1.3.

We also performed a flow field analysis for the evaporation processes corresponding to different ε_{sf}, and Fig. 3 gives the flow rates and flow directions at several typical intermediate states. In general, evaporation flux along the vapor-liquid interface (see the black dashed line in Fig. 3) is nonuniform. Roughly speaking, when the contact angle is lower than $\pi/2$ (namely, $\varepsilon_{sf} > 0.5$), the flux gradually increases from the top of the droplet to the triple contact line [16,33]. When the contact angle is greater than $\pi/2$, however, evaporation flux along the vapor-liquid surface has approximately the same value (Fig. 3), in good agreement with theoretical results [33].

In addition, the nonuniform evaporation flux induces the internal flow during the evaporation process. For droplets with a contact angle larger than $\pi/2$, the fluid inside the droplets flows from the contact line to the center of the droplet [see Fig. 3(a)], while for droplets with a contact angle smaller than $\pi/2$, the fluid near the contact line evaporates more rapidly than other regions. To maintain the fixed contact angle, a flow toward the contact line is created inside the droplet to compensate the fluid evaporated near the edge [see Figs. 3(b)–3(d)].

The flow field analysis in Fig. 3(c) also gives the detailed evaporation dynamics for the droplet with $\varepsilon_{sf} = 1.1$. Within the droplet, the flow field is the same as that of droplets for $\varepsilon_{sf} = 0.7$ and 1.3. However, within the monolayer film, the flow direction is almost parallel to the substrate surface, which indicates that the fluid inside the film evaporates mainly at the film edge, rather than the vapor-liquid interface. As shown in Fig. 1(c), the film lasts for a time of $\sim 1000 w_0$ after the disappearance of the upper droplet, which results in a longer droplet lifetime (see Fig. 2).

B. Evaporating droplets on rough substrates

For a real substrate, there exist different types of roughness at the nanometer scale. Now we study how the nanoscale roughness influences the evaporating modes, and to simplify the question, a geometric, ring-patterned roughness is introduced to coat the flat substrate [see Fig. 4]. This kind of patterned roughness has been successfully employed to illustrate the stability of nanobubbles [32]. Here we considered two saturation levels: one is set to RH = 70% as above and the other is set to RH = 102%, which is slightly supersaturated but insufficient to induce the growth of nanodroplets. ε_{sf} is set to 0.3 and 0.7, respectively, corresponding to the hydrophobic and hydrophilic substrates.

The time evolution of droplet volume is shown in Fig. 4(e), which indicates that most nanodroplets keep evaporating and ultimately disappear. In the case of RH = 70% and $\varepsilon_{sf} = 0.3$, the nanodroplet tends to evaporate in the mixed mode with a CCL-CCA transition taking place at the early stage

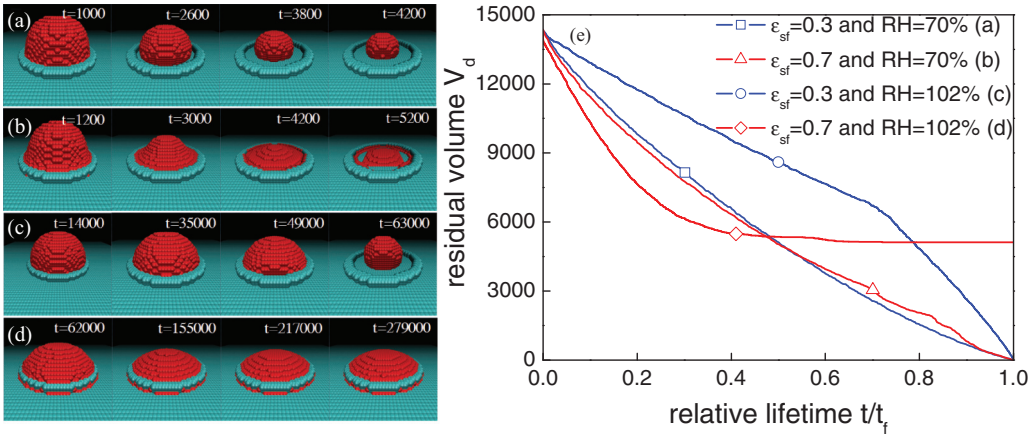

FIG. 4. (Color online) Time evolution of evaporating droplets upon rough substrates. Typical snapshots of evaporating droplets upon rough substrates with (a) $\varepsilon_{sf} = 0.3$ and RH = 70%, (b) $\varepsilon_{sf} = 0.7$ and RH = 70%, (c) $\varepsilon_{sf} = 0.3$ and RH = 102%, and (d) $\varepsilon_{sf} = 1.7$ and RH = 102%. (e) The residual volume V_d versus relative time t/t_f of evaporating droplets upon rough substrates.

[see Fig. 4(a)]. While under the conditions of $\varepsilon_{sf} = 0.7$ and RH = 70%, the stronger fluid-substrate interaction induces the pinning of the contact line to the ringlike roughness. However, the contact line pinning alone would not be able to stabilize the nanodroplet. As a result, the droplet evaporates always in the CCL mode with the contact line pinning [see Fig. 4(b)], and would finally disappear due to the nonequilibrium nature of the vapor-liquid interface [see Fig. 5(a)]. This observation indicates that although contact line pinning can block the evaporation from the triple contact line, the nonequilibrium nature of the vapor-liquid interface would cause the nanodroplets to become unstable.

Then, we increase the RH to 102% at which the vapor is weakly supersaturated. Again, in the case of $\varepsilon_{sf} = 0.3$ and RH $\sim$ 102% the droplet evaporates and ultimately disappears in the mixed mode [see Fig. 4(c)], and the time for the CCL-CCA transition corresponds to the turning point in the curve of volume evolution [see Fig. 4(e)]. This stage of the CCL mode has a much longer time than that at $\varepsilon_{sf} = 0.3$ and RH = 70%, which suggests that the CCL-CCA transition also depends on the supersaturation. Although the droplet is again unstable, the much longer lifetime [see Figs. 4(a) and 4(c)] indicates that as RH increases from 70% to 102%, the evaporation flow rate through the vapor-liquid interface slows down considerably.

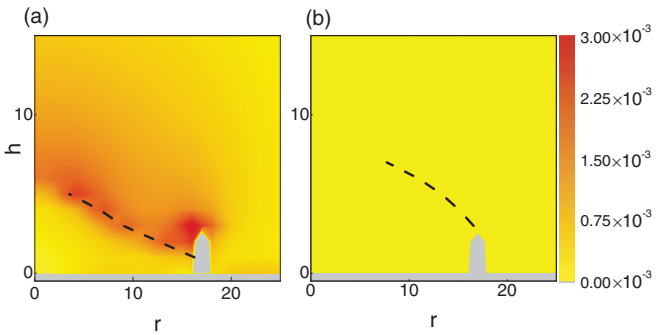

FIG. 5. (Color online) The flow rate of evaporating droplets upon rough substrates: (a) $\varepsilon_{sf} = 0.7$ and RH = 70% at $t = 4200$, and (b) $\varepsilon_{sf} = 0.7$ and RH = 102% at $t = 217\,000$. The black dashed line represents the vapor-liquid interface. The corresponding snapshots are given in Fig. 4.

It is surprising that in the case of RH = 102% and $\varepsilon_{sf} = 0.7$, the droplet volume remains unchanged after an initially rapid evaporation [Fig. 4(e)], indicating that the nanodroplet becomes stable. Figure 4(d) confirms that the droplet evaporates initially in the CCL mode and then becomes a stable nanodroplet. The unexpected stability of nanodroplets is here ascribed to the contact line pinning and equilibrium nature of the vapor-liquid interface, similar to that for nanobubble stability [32]. Another interesting observation is that the stable nanodroplet [see Fig. 4(d)] typically has a contact angle different from that on the smooth surface [see Fig. 1(b)], showing that the contact angles for stable nanodroplets are independent of the substrate chemistry. This observation is reminiscent of the substrate chemistry independence of the nanobubble contact angle [9,12,32], and again demonstrates the similarity between the stability of nanobubbles and that of nanodroplets.

The stability of the nanodroplet in the case of RH = 102% and $\varepsilon_{sf} = 0.7$ is confirmed by the zero evaporation rate on the liquid-vapor interface [Fig. 5(b)], which demonstrates that the liquid-vapor interface reaches equilibrium. This observation indicates that the nanodroplet is a part of a critical nucleus. If and only if the nanodroplet is a critical nucleus or a part of a critical nucleus for which the fluid molecules condensing onto the droplet are exactly balanced by those evaporating from it, the net evaporation rate is zero [Fig. 5(b)]. Moreover, the abnormal stability and relatively smaller contact angle indicate that the nanodroplet is not a critical nucleus for heterogeneous nucleation. Instead, the nanodroplet is identified as a part of the critical nucleus for homogeneous nucleation. Although the equilibrium between a critical nucleus for homogeneous nucleation and its surrounding vapor is an unstable one, if the contact line is pinned, the nucleus becomes stable, as explained below.

In our previous work [32], we have proved that the pinning effects can induce nanobubble stability. In the case of nanodroplets, similarly, the roughness of substrates provides a pinning force on the three-phase contact line and causes the

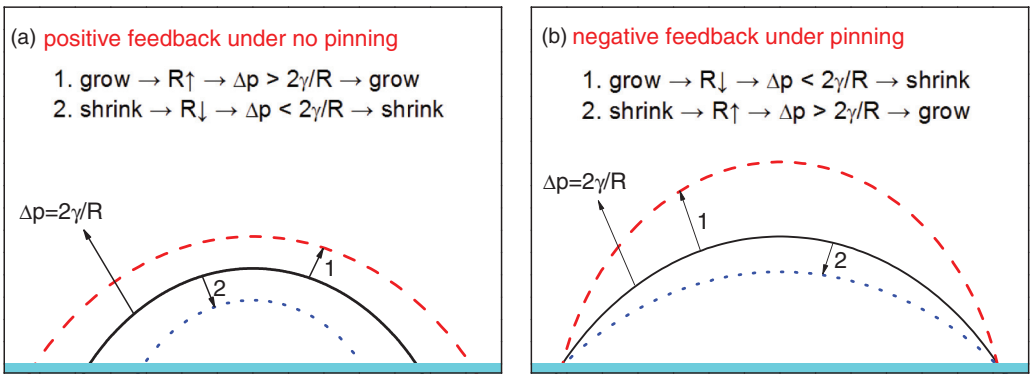

FIG. 6. (Color online) Schematic illustration of the positive feedback mechanism for unstable nanodroplets without contact line pinning (a) and that of the negative feedback mechanism for stable nanodroplets under contact line pinning (b). The black solid lines indicate the equilibrium vapor-liquid interface, and the dashed and dotted lines represent the unequilibrium vapor-liquid interface.

contact line pinning. Figure 6 gives the mechanism of how nanodroplets are stabilized. The classical nucleation theory (CNT) suggests that the free energy cost for the formation of a droplet in the bulk phase includes two terms, $\Delta\Omega = -\frac{4}{3}\pi R^3 \Delta p + 4\pi R^2 \gamma_{lv}$, with R the droplets radius, Δp the pressure difference between the liquid and the vapor, and γ_{lv} the vapor-liquid surface tension. Therefore, the radius of the critical nucleus R_c can be obtained by minimizing above free energy [34] and expressed as $R_c = 2\gamma_{lv}/\Delta p$, which is the same as the Laplace equation. For the critical nuclei, the contribution of energy cost from Δp, which tends to make the droplet grow, is balanced by that from γ_{lv}, which makes the droplet shrink.

As shown in Fig. 6(a), the equilibrium droplet on substrates without contact line pinning has two destinies: If the droplet initially grows, the droplet radius will increase because the droplet tends to keep its contact angle constant. Thus, $2\gamma_{lv}/R$ decreases and $\Delta p > 2\gamma_{lv}/R$, and the droplet would keep growing and finally results in the vapor-to-liquid phase transition. If the droplet initially shrinks, the droplet radius will decrease and $2\gamma_{lv}/R$ increases. Hence, $\Delta p < 2\gamma_{lv}/R$, and the droplet will keep shrinking and thus induce the disappearance of the nanodroplet. As a result, this positive feedback mechanism can rapidly lead to the growth or disappearance of the small droplet. Therefore, nanodroplets are not stable if no contact line pinning is imposed by the substrates.

However, the situation is different for an equilibrium nanodroplet with contact line pinning [see Fig. 6(b)]. Note that the line tension may contribute substantially to the free energy of the nanodroplet [35] Ω, but it does not affect $\Delta\Omega$ under the condition of contact line pinning. This is because the resultant force of the lateral forces on the contact line must be zero for a static contact line. If the droplet grows, the droplet radius will decrease because the contact line cannot move, and $2\gamma_{lv}/R$ increases accordingly. Thus, $\Delta p < 2\gamma_{lv}/R$, and the droplet will shrink to the equilibrium state. If, on the other hand, the droplet shrinks, the droplet radius will increase, and thus $\Delta p > 2\gamma_{lv}/R$, leading to the growth of the droplet. It is the negative feedback mechanism caused by the contact line pinning that prevents the nanodroplet from shrinking and growing, thus stabilizing the nanodroplet.

In general, stable nanodroplets were predicted from our calculations under the conditions of low vapor supersaturation and contact line pinning. The flow field analysis shows a zero evaporation rate for the stable nanodroplets on the liquid-vapor interface, indicating that the nanodroplets are part of critical nuclei of homogeneous nucleation. The stability of the nanodroplet can be interpreted within the framework of CNT, and a negative feedback mechanism caused by contact line pinning and supersaturated vapor environment is proposed in this work.

IV. CONCLUSION

A liquid droplet sitting on substrate in an open system is usually assumed to be thermodynamically unstable, and will eventually either evaporate or grow. However, the accumulated evidence for the existence of a stable nanobubble, the counterpart of a nanodroplet, poses a question of whether nanodroplets are stable. From the aspect of evaporation dynamics, in this work we revisit the stability of nanodroplets upon smooth and rough substrates, using the KLDFT method.

On smooth substrates, the droplet was found to evaporate generally in the CCA mode, with a contact angle non-monotonously depending on the fluid-substrate interaction. For smooth substrates with a strong fluid-substrate attraction, a monolayer liquid film on which the droplet sits is formed, affecting the contact angle and the evaporation dynamics. The liquid monolayer usually evaporates differently: It evaporates much more slowly than the droplet sitting on substrates or remains stable during the evaporation process.

On rough substrates, the droplets evaporate in the CCL mode or the CCL-CCA mixed mode. The reason for the existence of a CCL stage is the local pinning force at the triple contact line induced by nanoscale roughness or chemical heterogeneity [32]. In an evaporating process, if a pinning-depinning transition occurs, the nanodroplet evaporates in the mixed mode with a CCL-CCA transition. Otherwise, it evaporates in the CCL mode.

Interestingly, stable nanodroplets sitting on rough substrates were found from our calculations if the vapor environment is weakly supersaturated and the contact line is pinned. For those stable nanodroplets, the equilibrium nature of the vapor-liquid interface indicates that the nanodroplets are part of a critical nucleus of homogeneous nucleation.

Furthermore, the unstable nucleus with the equilibrium vapor-liquid interface is stabilized by the contact line pinning. The stability of the nanodroplet can be interpreted within the framework of classical nucleation theory, and a negative feedback mechanism caused by contact line pinning is proposed in this work.

Our prediction on the existence of stable nanodroplets can be tested in future experiments and simulations. Our model gives the prerequisites for the existence of stable nanodroplets, i.e., contact line pinning caused by physically rough and/or chemically heterogeneous substrates and supersaturated vapor at a low level of supersaturation. Experiment techniques on the formation of stable nanobubbles may also be helpful to produce stable nanodroplets: solvent exchange technique to establish a supersaturated environment [8] and substrates to produce contact line pinning effect [36]. As is well known, surfaces with regularly spaced roughness can be fabricated in the nanometer to micrometer range, thus permitting control over the size scale of the tiny droplets. This has important technological implications for creating well-defined nanodroplets. On a more fundamental level, our prediction of stable nanodroplets uncovers a rich phase behavior for fluids on the rough surfaces, and enhances our understanding of the wetting properties of substrates and the long-ranged interaction between two neighboring substrates.

ACKNOWLEDGMENTS

This work is supported by National Natural Science Foundation of China (Grant No. 21276007). The authors thank CHEMCLOUDCOMPUTING of BUCT, and the Supercomputing Center, CNIC, CAS for providing computer time.

[1] M. Nosonovsky and B. Bhushan, Nano Lett. **7**, 2633 (2007).
[2] X. Chen, R. Ma, J. Li, C. Hao, W. Guo, B. L. Luk, S. C. Li, S. Yao, and Z. Wang, Phys. Rev. Lett. **109**, 116101 (2012).
[3] T. P. Bigioni, X. Lin, T. Nguyen, E. Corwin, T. A. Witten, and H. M. Jaeger, Nat. Mater. **5**, 265 (2006).
[4] C. Sodtke and P. Stephan, Int. J. Heat Mass Transf. **50**, 4089 (2007).
[5] T. Kawase, H. Sirringhaus, R. H. Friend, and T. Shimoda, Adv. Mater. **13**, 1601 (2001).
[6] I. Barbulovic-Nad, M. Lucente, Y. Sun, M. Zhang, A. R. Wheeler, and M. Bussmann, Crit. Rev. Biotechnol. **26**, 237 (2006).
[7] B. Sobac and D. Brutin, Phys. Rev. E **84**, 011603 (2011).
[8] Z. Q. Ouyang, Y. Zhang, X. J. Li, J. Hu, M. Q. Li, and F. J. Yang, J. Vac. Sci. Technol. B **18**, 2573 (2000).
[9] N. Ishida, T. Inour, M. Miyahara, and K. Higashitani, Langmuir **16**, 6377 (2000).
[10] R. Steitz, T. Gutberlet, T. Hauss, B. Klösgen, R. Krastev, S. Schemmel, A. C. Simonsen, and G. H. Findenegg, Langmuir **19**, 2409 (2003).
[11] M. Switkes and J. W. Ruberti, Appl. Phys. Lett. **84**, 4759 (2004).
[12] L. J. Zhang, X. H. Zhang, C. H. Fan, Y. Zhang, and J. Hu, Langmuir **25**, 8860 (2009).
[13] J. W. Yang, J. M. Duan, D. Fornasiero, and J. Ralston, J. Phys. Chem. B **107**, 6139 (2003).
[14] X. H. Zhang, N. Maeda, and V. S. J. Craig, Langmuir **22**, 5025 (2006).
[15] X. H. Zhang, A. Quinn, and W. A. Ducker, Langmuir **24**, 4756 (2008).
[16] R. D. Deegan, O. Bakajin, T. F. Dupont, G. Huber, S. R. Nagel, and T. A. Witten, Nature (London) **389**, 827 (1997).
[17] S. Maheshwari, L. Zhang, Y. Zhu, and H. Chang, Phys. Rev. Lett. **100**, 044503 (2008).
[18] X. Shen, C. Ho, and T. Wong, J. Phys. Chem. B **114**, 5269 (2010).
[19] B. J. Fischer, Langmuir **18**, 60 (2002).
[20] H. Hu and R. G. Larson, J. Phys. Chem. B **106**, 1334 (2002).
[21] D. Golovko, H. Butt, and E. Bonaccurso, Langmuir **25**, 75 (2009).
[22] D. Orejon, K. Sefiane, and M. E. R. Shanahan, Langmuir **27**, 12834 (2011).
[23] H. M. Gorr, J. M. Zueger, and J. A. Barnard, Langmuir **28**, 4039 (2012).
[24] J. Kim, S. I. Ahn, J. H. Kim, and W. Zin, Langmuir **23**, 6163 (2007).
[25] G. Mchale, S. M. Rowan, M. I. Newton, and M. K. Banerjee, J. Phys. Chem. B **102**, 1964 (1998).
[26] G. Li, S. M. Flores, C. Vavilala, M. Schmittel, and K. Graf, Langmuir **25**, 13438 (2009).
[27] T. Furuta, A. Nakajima, M. Sakai, T. Isobe, Y. Kameshima, and K. Okada, Langmuir **25**, 5417 (2009).
[28] K. R. Khedir, G. K. Kannarpady, H. Ishihara, J. Woo, S. Trigwell, C. Ryerson, and A. S. Biris, J. Phys. Chem. C **115**, 13804 (2011).
[29] P. A. Monson, J. Chem. Phys. **128**, 084701 (2008).
[30] Y. Men, X. Zhang, and W. Wang, J. Chem. Phys. **131**, 184702 (2009).
[31] J. R. Edison and P. A. Monson, J. Low Temp. Phys. **157**, 395 (2009).
[32] Y. Liu and X. Zhang, J. Chem. Phys. **138**, 014706 (2013).
[33] T. A. H. Nguyen and A. V. Nguyen, Langmuir **28**, 1924 (2012).
[34] Y. Men and X. Zhang, J. Chem. Phys. **136**, 124704 (2012).
[35] Y. Liu, J. Wang, and X. Zhang, Sci. Rep. **3**, 2008 (2013).
[36] X. Zhang, D. Y. C. Chan, D. Wang, and N. Maeda, Langmuir **29**, 1017 (2013).